

# Double Exchange in Electron Doped $\text{Ca}_{1-x}\text{Y}_x\text{MnO}_3$ Manganites

H. Aliaga, M. T. Causa, H. Salva, M. Tovar, A. Butera and B. Alascio.  
*Centro Atómico Bariloche and Instituto Balseiro*  
*Comisión Nacional de Energía Atómica and Universidad Nacional de Cuyo.*  
*8400 San Carlos de Bariloche, Argentina.*

D. Vega, G. Polla, G. Leyva, and P. König  
*Centro Atómico Constituyentes.*  
*Comisión Nacional de Energía Atómica*  
*1650 San Martín, Buenos Aires, Argentina.*  
(January 10, 2019)

We have studied structural, magnetic and transport properties as a function of temperature and magnetic field in the electron doped manganite  $\text{Y}_x\text{Ca}_{1-x}\text{MnO}_3$ , for  $0 \leq x \leq 0.25$ . We found that in the paramagnetic regime, the magnetic susceptibility,  $\chi$ , deviates substantially from a Curie-Weiss law for  $x > 0$ . With a simple model where antiferromagnetic (AF) superexchange and ferromagnetic (FM) double exchange (DE) compete, we fit the experimental  $\chi(x, T)$  obtaining parameter values which indicate that the FM-DE interaction is about twice as intense as the AF interaction. In the ordered phase, the  $H$ -dependence of the magnetization  $M(x, T)$  is explained in terms of magnetic polarons. We propose that the displacement of the  $e_g$  electrons from one magnetic sublattice to other (in the G-type AF background) causes the alignment of the polaron with  $H$ . Signatures of polaronic behavior were also found in the  $x$  and  $T$  dependence of the electric resistivity.

PACS numbers: 75.30.Vn, 75.10.-b, 75.40.Mg

## I. INTRODUCTION

The existence of magnetoresistance (MR) in Mn oxides with perovskite structure was discovered at the very early stage of the study of the transition metal oxides<sup>1</sup>. The interest in these compounds has revived recently due to the discovery of very large MR ( $\sim 10^6\%$ ) which led to call this phenomenon colossal magnetoresistance (CMR). At the same time a magnetic field induced insulator-metal and structural transition<sup>2</sup> was also discovered. Most studies were devoted to the perovskite compounds  $\text{R}_x\text{A}_{1-x}\text{MnO}_3$  (R=trivalent rare earth and A=divalent alkaline earth) producing  $x \text{ Mn}^{3+}$  and  $(1-x) \text{ Mn}^{4+}$  ions, respectively. Ferromagnetic (FM) double-exchange (DE) interaction between localized  $t_{2g}$  Mn electron configuration, mediated by itinerant spin-polarized  $e_g$  electrons, is in the base of CMR. The concentration  $x$  is not the only parameter to be taken into account in CMR materials. Chemical parameters such as the average R-A cationic radius and the cationic size mismatch quantified by the variance  $\sigma^2$  of the ionic radii<sup>3,4</sup> are also relevant. The phase diagrams for  $\text{R}_x\text{A}_{1-x}\text{MnO}_3$  families were found to be non-symmetric and hole or electron doping cause disimilar effects. Theoretical studies<sup>5</sup> suggested at least three possible scenarios to understand the low electron doping region: i) Canting of the magnetic structure. ii) Phase separation into ferromagnetic and antiferromagnetic phases with charge separation. iii) Ferromagnetic polarons. Therefore, experiments on families of compounds, covering different ranges of physical and chemical parameters can be used to clarify this issue. The most studied series are those where A=Ca. In

Ref. 6 an analysis of the saturation magnetization ( $M$ ) of  $\text{Ca}_{1-x}\text{R}_x\text{MnO}_3$  was performed for different R ions. They found, in all cases, an initial rise of  $M$  with  $x$  followed by a sudden drop associated to charge ordering (CO). The value of  $x$  where the CO phase appears depends on the size of R: a higher electron concentration is necessary to establish the AF-CO state as the ionic radius of R decreases. In this paper we study structural, transport, and magnetic properties of  $\text{Ca}_{1-x}\text{Y}_x\text{MnO}_3$ . Trivalent Y is one of the smallest ions synthesizing in the perovskite structure. Then the charge ordering phase is expected for higher  $x$  in comparison with the compounds studied in Ref. 6 and a more detailed analysis of the initial magnetic phase can be made. The Y series synthesizes<sup>7</sup> with orthorhombic structure for  $0 < x < 0.8$ . Magnetoresistance effects were reported<sup>8</sup> for  $0.05 \leq x \leq 0.15$ , indicating the presence of DE interaction. The non magnetic character of Y ions makes the series  $\text{Ca}_{1-x}\text{Y}_x\text{MnO}_3$  an excellent system to study the evolution of the magnetism of Mn ions, without interference from other magnetic species. This is specially important in the paramagnetic regime. We present here magnetic measurements in the region  $0 \leq x \leq 0.25$  and compare with the resistivity. We analyse these measurements in the PM and ordered phases to show that they can be understood in terms of small magnetic polarons<sup>9</sup> arising from the DE mechanism between  $\text{Mn}^{4+}$  and  $\text{Mn}^{3+}$ . We will show that this model explains also experimental results reported in the literature<sup>4,6,10-13</sup> for  $\text{Ca}_{1-x}\text{R}_x\text{MnO}_3$  with  $x$  values covering the electron doped region and R different from Y.

## II. EXPERIMENTAL

Ceramic polycrystalline samples of  $\text{Ca}_{1-x}\text{Y}_x\text{MnO}_3$  were prepared by solid state reaction methods<sup>7,8</sup>. Room temperature x-rays diffractograms show that  $\text{CaMnO}_3$  crystallizes in an orthorhombic  $Pnma$  cell with parameters  $a=5.284(5)\text{\AA}$ ,  $b=7.453(5)\text{\AA}$ , and  $c=5.266(5)\text{\AA}$ . For  $0 \leq x \leq 0.25$  all the samples crystallize in single orthorhombic phase O (with  $c < b/\sqrt{2}$ ). In Fig. 1 we show the variation of the cell parameters in the range studied here. The structural distortion increases with  $x$  and can be evaluated by the orthorhombic strain:  $s = 2(a-c)/(a+c)$ , shown in the inset of Fig. 1. The tilt and rotation angles, produced respectively by apical and planar oxygens shift, remains approximately constant. A study of the cell parameters evolution with  $T$ , for  $x=0.07$ , shows no structural transition in the range 15-300K. Electrical resistivity was measured with the 4-probe method using a current source of 10–100 $\mu\text{A}$ . The dc-magnetization  $M$  was measured with a SQUID magnetometer between 5K and 300K for  $H \leq 50\text{kOe}$  and with a Faraday Balance magnetometer between 300K and 1000K with  $H \leq 10\text{kOe}$ .

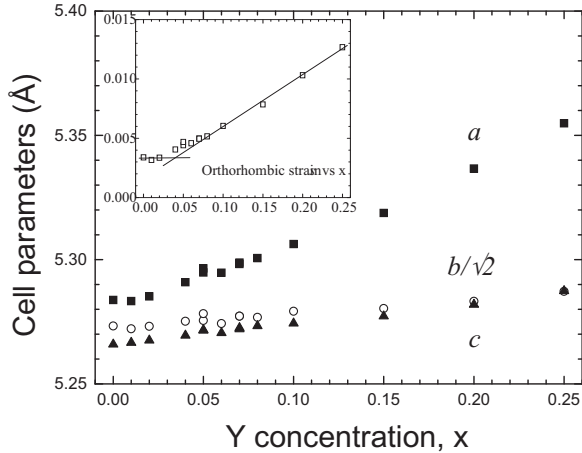


FIG. 1. Room temperature cell parameters  $a$ ,  $b$ , and  $c$  as a function of  $x$ . In the inset, the orthorhombic strain  $s$  vs.  $x$  is shown.

## III. RESULTS

In Fig. 2 we show  $H/M$  vs.  $T$  measured for the samples  $x = 0, 0.05, 0.07$ , and  $0.10$ . In all cases  $M$  is a linear function of  $H$  for  $T \geq 140\text{K}$ . A Van Vleck contribution is expected for  $\text{Mn}^{4+}$  ions<sup>14</sup>. In our measurements this contribution was subtracted in the paramagnetic phase, proportionally to  $(1-x)$ . The  $\text{CaMnO}_3$  data were fitted with a Curie Weiss law,  $\chi = C/(T-\Theta)$ , where  $C$  is the Curie constant and  $\Theta$  is the Curie-Weiss temperature, obtaining  $C = (1.95 \pm 0.05) \text{ emu-K/mol}$  (near the expected  $\text{Mn}^{4+}$  value 1.875) and  $\Theta \approx -400\text{K}$ . This value points to a strong antiferromagnetic (AF) superexchange interaction between  $\text{Mn}^{4+}$  ions. In this case

$M$  remains linear with  $H$  down to  $T_N$ . Using neutron diffraction, Wollan and Kohler<sup>15</sup> found G-type AF ordering below  $T_N \sim 123\text{K}$ . The ratio  $\Theta/T_N > 3$  is an indication of the importance of second neighbors interaction in the perovskite structure<sup>14</sup>. Further magnetic measurements have shown the existence of a weak ferromagnetic moment<sup>16</sup> below  $T_N$  of  $M_{WF} \sim 0.03\mu_B/\text{Mn}$  ion, associated with Dzialoshinsky-Moriya (DM) interaction. The hysteresis loop for this weak ferromagnetic component shows a small coercive field ( $H_c = 0.12\text{T}$  at 5K). Since the reversal of  $M_{WF}$  implies reversal of the full lattice magnetizations, the  $H_c$  observed suggest a small anisotropy energy.

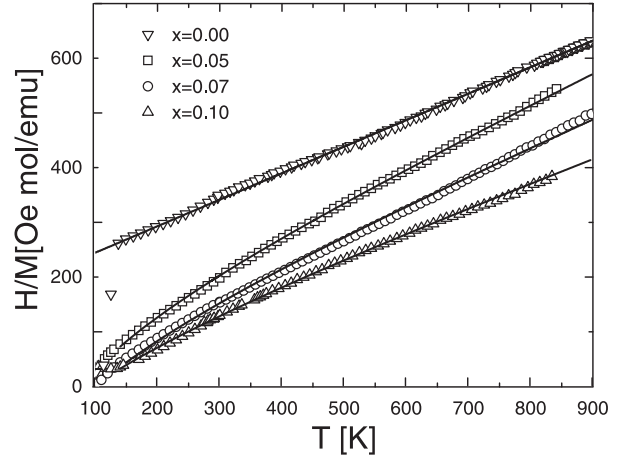


FIG. 2. Measured  $\chi^{-1}(T)$  curves (symbols) with  $H=10\text{kOe}$  and calculated (lines) for the samples  $x = 0, 0.05, 0.07$  and  $0.10$ . Notice the deviation from a Curie-Weiss law below  $\approx 450\text{K}$ .

At high temperatures, the samples with  $x > 0$  also follow a Curie-Weiss law. However, for  $T \lesssim 450\text{K}$   $H/M$  deviates substantially from this behaviour. In Fig. 3(a) it is shown the dependence of  $\Theta$  with the doping  $x$ , as obtained from high  $T$  fits. Small  $Y$  doping causes large changes in the  $\Theta$  values, indicating an evolution from a strong AF for  $x=0$  ( $\Theta \approx -400\text{K}$ ) to a FM one for  $x \approx 0.10$  ( $\Theta \approx +80\text{K}$ ). In Fig. 4 we show  $M$  vs.  $T$  curves measured with  $H = 5\text{kOe}$ , for selected samples. Below  $T \sim 125\text{K}$  a FM component that increases with  $x$  up to  $x = 0.10$  was measured. A magnetic transition temperature,  $T_{mo}$ , was defined as the temperature with maximum slope of  $M(T)$ . A detailed dependence of  $T_{mo}$  vs.  $x$  is shown in Fig. 3(b).

In Fig. 5 we show  $M$  vs.  $H$  at  $T = 5\text{K}$ . At low fields ( $H < 5\text{kOe}$ ),  $M(H)$  varies rapidly with  $H$  and, for  $H=0$  there is only a small remanent magnetization. For  $|H| \gtrsim 30\text{kOe}$ ,  $M(H)$  can be approximated by:  $M = M_0 + \chi_{diff} H$ , where  $M_0$  is the ferromagnetic contribution to  $M$  and  $\chi_{diff}$  is the high field differential susceptibility. In the case of  $x=0$ ,  $M_0 = M_{WF}$  is the DM contribution and  $\chi_{diff}$  is the AF susceptibility. Measurements between 5K and  $T_N$  shows that  $\chi_{diff}(T)$  remains

almost constant, after subtraction of a small Curie-type contribution observed below 25K (equivalent to about 0.3% of  $\text{Mn}^{4+}$  free ions).

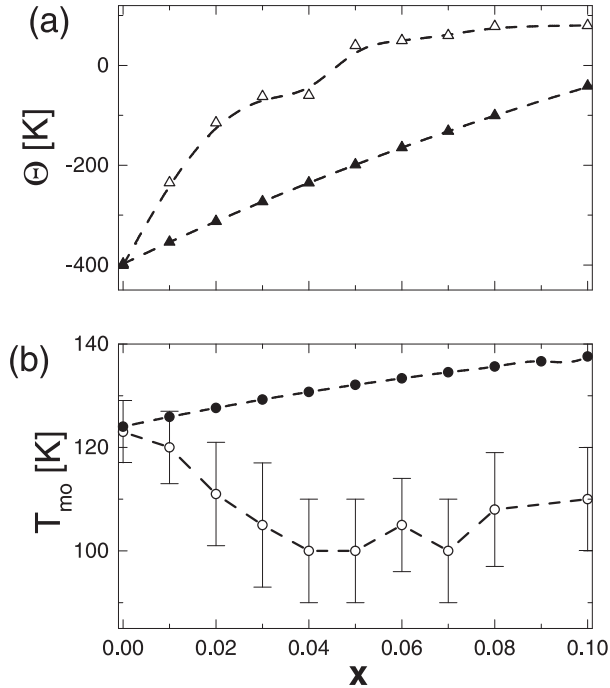


FIG. 3. (a) Curie-Weiss temperatures,  $\Theta$  vs.  $x$ . Open symbols are determined from linear fits above 500K. Solid symbols are derived from Eq. 7. (b) Measured (open) and calculated (solid) magnetic ordering temperature,  $T_{mo}$  vs.  $x$ .

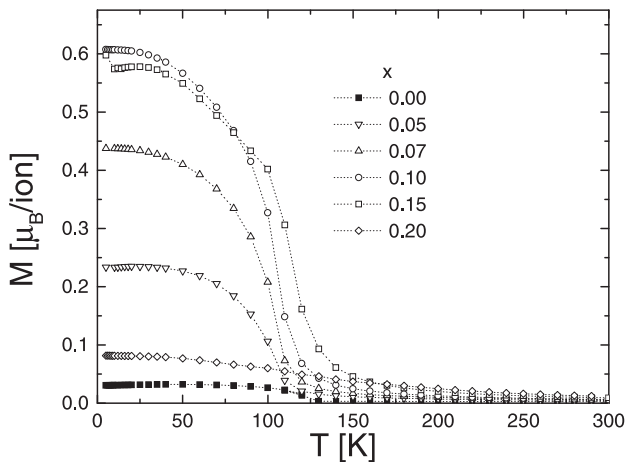


FIG. 4.  $M$  vs.  $T$  curves with  $H=5\text{kOe}$ . Lines are guides to the eye.

For  $x > 0$  a similar behaviour was observed at all temperatures measured, with an important increase of both  $M_0$  and  $\chi_{diff}$ . We have measured in detail the temperature dependence of  $M$  vs.  $H$  for  $x=0.1$ . The resulting  $M_0(T)$  and  $\chi_{diff}(T)$  are compared in Fig. 6 with the case  $x=0$ . The susceptibility  $\chi_{diff}(T)$  shows a maximum in coincidence with  $T_{mo}$ . This behaviour resembles that of

an antiferromagnet, although with a much large susceptibility than that of the undoped  $\text{CaMnO}_3$ .

In Fig. 7(a) we plot  $M_0$  vs.  $x$  at 5K. Notice that  $M_0$  is much smaller than the expected value for full FM alignment ( $M_S \sim 3\mu_B/\text{Mn ion}$ ). In the region  $0 \leq x \leq 0.03$ ,  $M_0(x)$  increases almost linearly, with an initial slope of  $\sim 0.85\mu_B/\text{Mn ion}$ . For  $x \gtrsim 0.03$ ,  $M_0$  increases more rapidly and reaches a maximum ratio  $M_0/x \approx 7.1\mu_B/\text{Mn ion}$  for  $x \sim 0.07-0.1$ . For  $x > 0.15$ ,  $M_0$  decreases sharply.

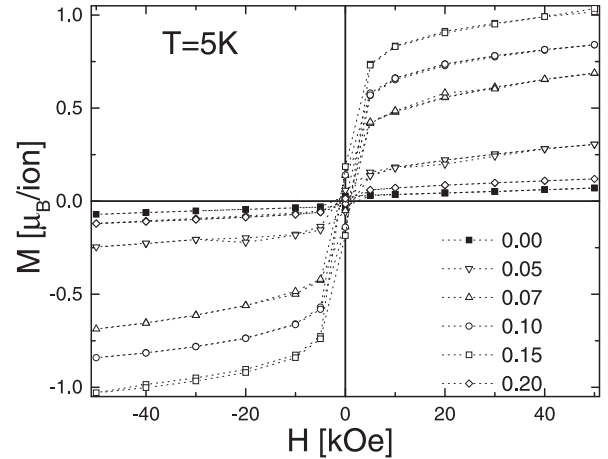


FIG. 5.  $M$  vs.  $H$  curves at 5K. Full alignment ( $M_0 \sim 3\mu_B$ ) is not reached in any case. Dotted lines are guides to the eye.

In Fig. 8(a) we present results for the resistivity in the range 4-300K. The sample  $x=0$  is the most resistive one, and a strong decrease in  $\rho$  is induced with small electronic doping  $x$ . Small features are found in  $\rho(T)$  near  $T_{mo}$ . These curves were fitted in the range 100-300K assuming a polaronic behaviour  $\rho(T) \propto T \exp[-\Delta/k_B T]$ , showing double exchange effects and activation energies of 1160, 390, 420, 490, 460, and 455K for the samples  $x=0, 0.01, 0.03, 0.05, 0.08$  and  $0.10$ , respectively. The dependence of  $\rho(T)$  in the range  $4\text{K} \leq T \leq 100\text{K}$ , is more complicated and shows a decrease of  $\ln \rho/dT$  at low  $T$ . This behaviour indicates that the material is not an insulator.

In Fig. 7(b) we present the dependence of the electric resistivity  $\rho(5\text{K})$ . The resistivity decreases orders of magnitude between  $x=0$  and  $x=0.05$ , remains almost constant for  $0.05 \leq x \leq 0.15$ , and then increases again for  $0.15 \leq x \leq 0.25$ . Comparing Figs. 7(a) and 7(b) in the range  $0 \leq x \leq 0.15$ , we see that the greater the concentration of carriers, the greater the conductivity and the magnetic moment. Fig. 8(b) shows the linear dependence found for the conductivity,  $\sigma$  vs.  $x$ . This result is in qualitative agreement<sup>17</sup> with the DE mechanism. In the region  $0.15 \leq x \leq 0.25$ , the resistivity increases and the magnetic moment decreases, the DE mechanism is broken, leading to a low magnetic moment-insulator state.

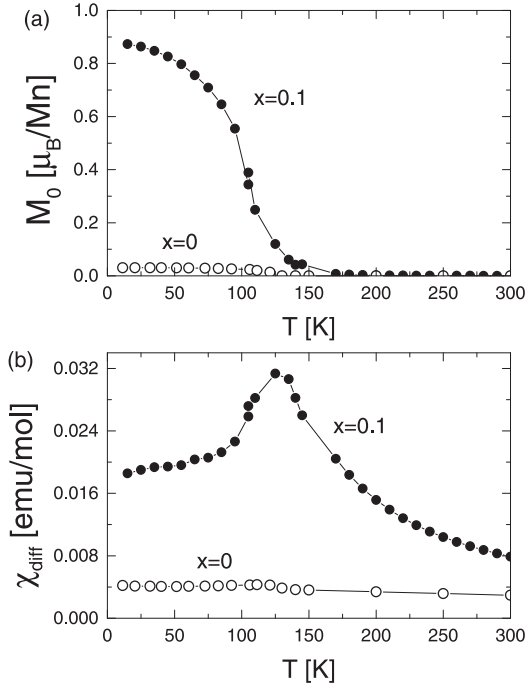


FIG. 6. T dependence of: (a)  $M_0$  and (b)  $\chi_{diff}$ , for  $x=0$  and 0.1, obtained from  $M$  vs.  $H$  in the high field linear regime.

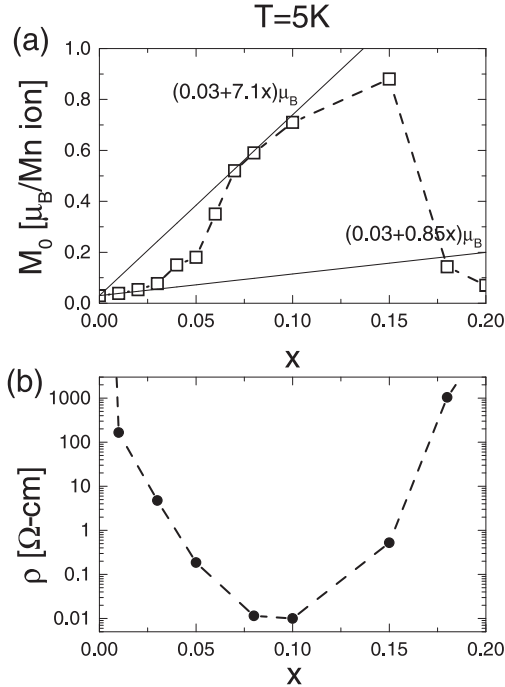


FIG. 7. (a) High field extrapolated magnetization  $M_0$  vs.  $x$ . Continuous straight lines indicates the initial and maximum slopes. (b) The zero field resistivity  $\rho$  vs.  $x$ . Notice the strong correlations between magnetism and resistivity. Dotted lines are guides to the eye.

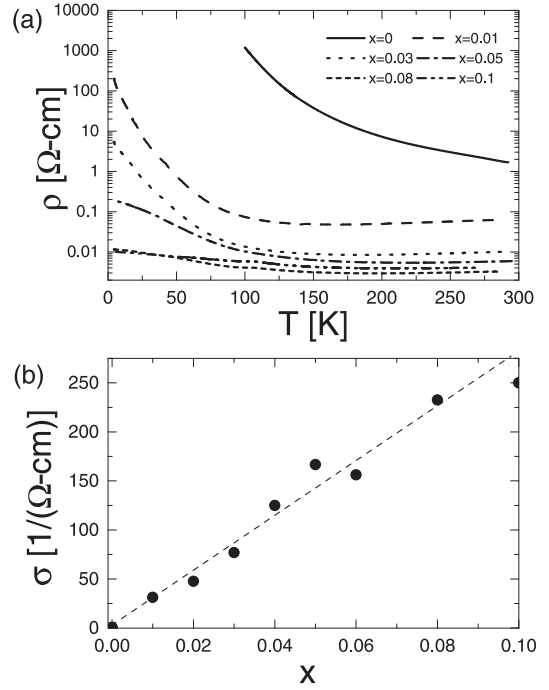


FIG. 8. (a)  $\rho$  vs.  $T$  for the samples  $x=0, 0.01, 0.03, 0.05, 0.08, 0.1,$  and  $0.15$ . (b)  $\sigma$  vs.  $x$  at 300K.

#### IV. DISCUSSION

When  $Y^{3+}$  substitutes for  $Ca^{2+}$  in  $CaMnO_3$ ,  $e_g$  electrons are introduced in the system. These electrons polarize the otherwise G-type AF background, forming magnetic polarons<sup>9</sup>. In the very dilute region, we expect that Jahn-Teller distortions surrounding each  $Mn^{3+}$  will tend to localize the  $e_g$  electrons, forming a combined lattice-magnetic polaron. In this regime each polaron carries an extra magnetic moment due to the added  $e_g$  electron ( $S=1/2$ ). Within this model the large variation of  $M$  with  $H$  for  $|H| \leq 10kOe$  (see Fig. 5) at low temperatures is mainly due to the alignment of these small polarons<sup>11</sup>. With zero applied field the  $Mn^{3+}$  spins, with a magnetic of  $4\mu_B$ , are oriented in random up and down directions in the lattice and the total average moment is null. With a nonzero field, polarons may easily reorient themselves parallel to the field, through the hopping of the  $e_g$  electron to a neighboring site using the DE mechanism. Fig. 9(a) sketches the suggested behaviour in the presence of a field  $H$ . This process results in a linear dependence:  $M_0/x \sim 1\mu_B/Mn$  ion.

Neutron diffraction experiments<sup>18</sup> show that, in the case of  $Ca_{1-x}Bi_xMnO_3$ , an essentially G-type AF background is preserved up to  $x \sim 0.1$ . We assume a similar scenario for  $Ca_{1-x}Y_xMnO_3$  since the lattice presents the same  $Pnma$  structure for the whole composition range of our samples. Small distortions of the perfect AF alignment are produced by the DE interactions, allowing the excitations of the  $e_g$  electrons from the localized Jahn-Teller states to a narrow conduction band, improving in

this way, the electrical conductivity.

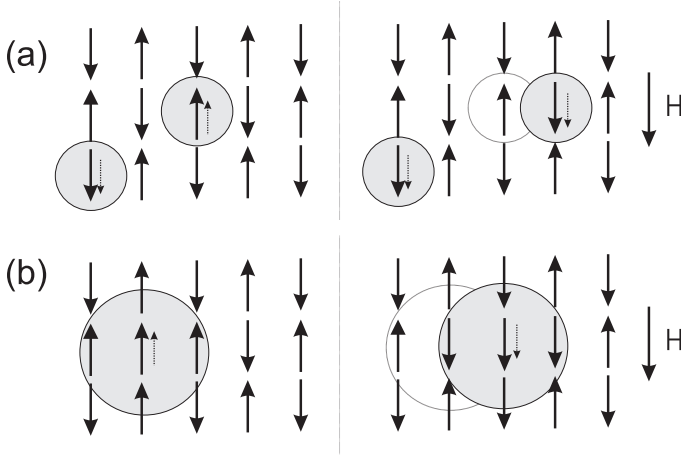


FIG. 9. (a) Each  $e_g$  electron added to the system couples ferromagnetically with the localized spin  $t_{2g}$  forming single-site polarons for small  $x$ . (b) For larger  $x$ , the size of the polarons increases, involving the neighborings Mn spins. spin-flip processes. The figure illustrates the proposed mechanism of magnetization reversal, with an applied field, through the hopping of  $e_g$  electrons.

For  $0.03 \lesssim x \lesssim 0.07$ , the  $M_0$  vs.  $x$  curve displays a pronounced concavity. For  $x \geq 0.07$ , we find again a linear regime with  $M_0/x \sim 7.1\mu_B/\text{Mn-ion}$ , indicating that the polarons carry a larger magnetic moment.

Changes in the  $x$  dependence of  $M_0$  may be due to the occupancy of states above the bottom of the band<sup>19</sup>, to effective interaction between polarons, or to variations of the crystallographic structure, that may favour different magnetic arrangements. The x-ray diffractograms show that all the samples may be indexed in the same orthorhombic O-phase at room temperature and no structural transitions has been observed between 15K and 300K for  $x=0.07$ . Thus we have discarded the appearance of magnetic phases (A- or C-like) other than the distorted G-type, since these phases have been observed for higher electron doping<sup>20</sup>, and associated with structural transitions<sup>21</sup> as in  $\text{Ca}_{0.85}\text{Sm}_{0.15}\text{MnO}_3$ . We can interpret the results in the region  $0.07 \lesssim x \lesssim 0.15$  with the following model: each  $\text{Mn}^{3+}$  couples ferromagnetically with the  $\text{Mn}^{4+}$  neighbors, after a spin flip process in the G-type AF lattice, see Fig. 9(b). This ferromagnetic coupling is favoured by the kinetic energy gain due to the hopping of the  $e_g$  electron into the neighboring localized spins, forming a larger magnetic polaron, comprising the  $\text{Mn}^{3+}$  site and its nearest neighbors. This process is made possible by the larger orthorhombic distortion of the whole lattice (Fig. 1) that provides distorted  $\text{Mn}^{4+}$  sites where the  $e_g$  electrons may jump more easily. With zero applied field, these polarons, are randomly oriented. When a magnetic field  $H$  is applied, the  $e_g$  electrons of the misaligned  $\text{Mn}^{3+}$  spins hop to a  $\text{Mn}^{4+}$  neighbor, which has its neighbors oriented in the direction of  $H$ . After two spin-flip processes, see Fig. 9(b), the displaced polarons

are aligned with the field and  $M_0/x = 7\mu_B/\text{Mn-ion}$  is expected. The linear increase of  $M(H)$  observed at high fields for all concentrations, could be interpreted as due to the contribution of the AF background. However, notice that  $\chi_{diff}$  is much larger than the AF susceptibility measured for  $x=0$  (see Fig. 6). This fact suggest that the application of high magnetic fields enhances the response of the  $\text{Mn}^{4+}$  ions beyond the boundaries of the  $H=0$  polarons.

In the paramagnetic phase, the most peculiar feature observed is the deviation from the Curie-Weiss law, presenting a negative curvature of the  $\chi^{-1}(T)$  curves (Fig. 2). In order to describe this behaviour in simple terms, we consider the system as a mixture of  $\text{Mn}^{4+}$  and  $\text{Mn}^{3+}$  ions. Taking into account that the ordered state for  $x=0$  is a G-type antiferromagnet we divide the system into two interpenetrated sublattices  $a$  and  $b$ , where  $\text{Mn}^{4+}$  and  $\text{Mn}^{3+}$  are randomly distributed with concentrations  $(1-x)$  and  $x$ , respectively. In a mean field approximation we consider superexchange interactions with first and second neighbors, between  $\text{Mn}^{4+}$ - $\text{Mn}^{4+}$ ,  $\text{Mn}^{3+}$ - $\text{Mn}^{3+}$  and DE between  $\text{Mn}^{4+}$ - $\text{Mn}^{3+}$  pairs. The equations satisfied by the sublattice magnetizations are:

$$M_4^a T = C_4 [H + \gamma_{44}(1-x)M_4^b + \gamma'_{44}(1-x)M_4^a + \gamma_{43}xM_3^b + \gamma'_{43}xM_3^a] \quad (1)$$

$$M_4^b T = C_4 [H + \gamma_{44}(1-x)M_4^a + \gamma'_{44}(1-x)M_4^b + \gamma_{43}xM_3^a + \gamma'_{43}xM_3^b] \quad (2)$$

$$M_3^a T = C_3 [H + \gamma_{33}xM_3^b + \gamma'_{33}xM_3^a + \gamma_{43}(1-x)M_4^b + \gamma'_{43}(1-x)M_4^a] \quad (3)$$

$$M_3^b T = C_3 [H + \gamma_{33}xM_3^a + \gamma'_{33}xM_3^b + \gamma_{43}(1-x)M_4^a + \gamma'_{43}(1-x)M_4^b] \quad (4)$$

where subindexes 4 and 3 indicate  $\text{Mn}^{4+}$  and  $\text{Mn}^{3+}$  ions respectively, superindexes  $a$  y  $b$  correspond to the two sublattices, and  $\gamma_{ij}$  are the parameters describing the exchange coupling between  $M_i$  and  $M_j$ . Primed parameter indicate interaction with second neighbors. The total magnetization is given by:

$$M = \frac{1}{2} [(M_4^a + M_4^b)(1-x) + (M_3^a + M_3^b)x] \quad (5)$$

In the PM regime we take  $M_4^a = M_4^b$  and  $M_3^a = M_3^b$ . The behaviour of the reciprocal susceptibility  $\chi^{-1}(T)$  is a hyperbola and only three independent parameters ( $\gamma_{44} + \gamma'_{44}$ ,  $\gamma_{33} + \gamma'_{33}$  and  $\gamma_{43} + \gamma'_{43}$ ) are necessary to fit the experimental curves, since first and second neighbors contribution cannot be separated. Best fits of the experimental data are shown as continuous lines in Fig. 2, where an excellent agreement is observed. For  $x=0$  the solutions of Eqs. 1-4 correspond to a Curie-Weiss behaviour

with a characteristic temperature  $\Theta = C_4(\gamma_{44} + \gamma'_{44})$ . From the fit, we derived  $\gamma_{44} + \gamma'_{44} = -204$  mol/emu. For  $0 < x \leq 0.10$ , the contribution to the total magnetization of the  $Mn^{3+}$  ions is small compared to the contribution of the  $Mn^{4+}$  species. For this reason we expect great indetermination in  $(\gamma_{33} + \gamma'_{33})$ , if left as a free parameter. Thus we have taken as an approximate fixed value,  $(\gamma_{33} + \gamma'_{33}) = +73$  mol/emu, as obtained for the  $Mn^{3+}$ - $Mn^{3+}$  interaction<sup>14</sup> in the pseudo-cubic high temperature phase of  $LaMnO_3$ . Therefore, when fitting the data for  $x > 0$ , only  $(\gamma_{43} + \gamma'_{43})$  is kept as an adjustable parameter. We obtained  $+361$ ,  $+386$  and  $+310$  mol/emu for  $x = 0.05$ ,  $0.07$ , and  $0.10$ , respectively. We have found that these results are rather insensitive to the value assumed for the  $Mn^{3+}$ - $Mn^{3+}$  interaction, within the experimental uncertainty ( $\sim 10\%$ ), if we take  $-204$  mol/emu  $\lesssim (\gamma_{33} + \gamma'_{33}) \lesssim 73$  mol/emu. The  $(\gamma_{43} + \gamma'_{43})$  parameter is always positive and approximately two times larger than  $\gamma_{44} + \gamma'_{44}$ , denoting strong ferromagnetic coupling between  $Mn^{4+}$  and  $Mn^{3+}$  pairs. From now on, we use the average value  $(\gamma_{43} + \gamma'_{43}) = +350$  mol/emu for all  $x$ .

The high temperature asymptote of  $\chi^{-1}(T)$  has a Curie-Weiss form, with

$$C = (1-x)C_4 + xC_3 \quad (6)$$

and

$$\Theta = C^{-1}[(1-x)^2 C_4^2 (\gamma_{44} + \gamma'_{44}) + 2(\gamma_{43} + \gamma'_{43})x(1-x)C_3 C_4 + x^2 C_3^2 (\gamma_{33} + \gamma'_{33})] \quad (7)$$

In Fig. 3(a) we compare the values of  $\Theta$  derived from this equation with those determined from a linear fit between 500K and 850K. Notice that the measured  $\chi^{-1}(T)$  curves do not completely reach the asymptotic linear regime in the temperature range of the experiments.

Within the mean field approximation used, it is also possible to express the solutions of Eqs. (1)-(4) in terms of two separate contributions

$$\chi(T) = \frac{C_{AF}}{(T - \Theta_{AF})} + \frac{C_{FM}}{(T - \Theta_{FM})} \quad (8)$$

where, for  $x \ll 1$ ,

$$C_{AF} = (1-x)C_4 + xC_3(1 - \Gamma^2) \quad (9)$$

$$C_{FM} = xC_3\Gamma^2 \quad (10)$$

with

$$\Gamma = 1 - (\gamma_{34} + \gamma'_{34})/(\gamma_{44} + \gamma'_{44}) \quad (11)$$

and

$$\Theta_{AF} = -(1-x)C_4(\gamma_{44} + \gamma'_{44}) + xC_3 \frac{(\gamma_{34} + \gamma'_{34})^2}{(\gamma_{44} + \gamma'_{44})} \quad (12)$$

$$\Theta_{FM} = xC_3 \left[ (\gamma_{33} + \gamma'_{33}) - \frac{(\gamma_{34} + \gamma'_{34})^2}{(\gamma_{44} + \gamma'_{44})} \right] \quad (13)$$

Using the values of  $(\gamma_{ij} + \gamma'_{ij})$  previously obtained, we find  $\Theta_{AF} < 0$  and  $\Theta_{FM} > 0$ , corresponding to AF and FM behaviour respectively.

This picture shows a FM-like component of the magnetization proportional to  $x$  (Eq. 10). In the absence of  $Mn^{3+} - Mn^{4+}$  interaction, this contribution corresponds to isolated  $Mn^{3+}$  ions. The effect of FM-DE coupling enhances the magnetic moment of the  $Mn^{3+}$  ions ( $\Gamma > 1$ ), reflecting the magnetic polaron formation. Using the values derived from the fitting of  $\chi(T)$ , we obtained an effective moment for the polarons,  $\mu_{eff} = 2.71\mu_{eff}(Mn^{3+})$ . This result suggest that the effective number of  $Mn^{4+}$  neighbors involved in the paramagnetic polarons is  $z_{eff} \simeq 5$ .

In order to analyze the magnetic ordering temperature, Eqs. (1-4) must be solved for  $H = 0$ . The highest temperature that allows nontrivial solution for  $M_i$  corresponds to the magnetic transition  $T_{mo}$ . For  $x = 0$ , AF ordering is achieved for  $T_{mo} = C_4(-\gamma_{44} + \gamma'_{44})$ . The values  $\gamma_{44} = -134$  mol/emu and  $\gamma'_{44} = -71$  mol/emu are derived from the measured<sup>14</sup>  $T_N = 123$  K. The magnetic state found preserves the AF alignment between  $M_4^a$  and  $M_4^b$ . The  $Mn^{3+}$  ions are oriented FM with respect to their  $Mn^{4+}$  first neighbors, irrespective of the value assumed for the  $Mn^{3+}$ - $Mn^{3+}$  interaction. In this limit the ordering temperature is given by

$$T_{mo} \approx T_N(1-x) + (C_3 C_4 / T_N)(\gamma_{43} - \gamma'_{43})^2 x(1-x) \quad (14)$$

where  $T_N = T_{mo}(x=0)$ . The first term reflects the dilution of the  $Mn^{4+}$  lattice and the second the effect of  $Mn^{3+} - Mn^{4+}$  interactions. We have varied  $\gamma_{43}$  and  $\gamma'_{43}$  in order to reproduce the  $x$  dependence of  $T_{mo}$ , shown in Fig. 3(b). For  $\gamma_{43} = 215$  mol/emu and  $\gamma'_{43} = 135$  mol/emu, we found that  $T_{mo}$  increases continuously from  $x = 0$  to  $x = 0.1$ , where a value of 137 K is reached, reproducing the experimental tendency for  $x > 0.04$ . The initial decrease of  $T_{mo}$  cannot be included in this description with a unique set of parameters in Eq. (14).

## V. CONCLUSIONS

We have measured the temperature and magnetic field dependence of structural, magnetic and transport properties in the manganites  $Ca_{1-x}Y_xMnO_3$ , for  $0 \leq x \leq 0.25$ . Despite of the small cationic size of Y, and the large mismatch between Y and Ca, we have synthesized single phase material with orthorhombic structure. Strong correlation between magnetization and conductivity in the region  $0 \leq x \leq 0.15$  was found, allowing to conclude that DE mechanism is present in this compound.

From the  $M$  vs.  $H$  dependence we found that the saturation magnetization increases with the electron concentration, reaching for  $x = 0.1$ ,  $M_0 \sim 1\mu_B/\text{Mn-atom}$ , that is far from the value expected for full FM alignment,  $M_0 = (3+x)\mu_B$ . We have interpreted these results

in terms of magnetic polarons, and we propose that the response of  $M$  vs.  $H$  is due to the displacement of the  $e_g$  electrons from one magnetic sublattice to the other, causing the alignment of the polarons with the external field (Fig. 7).

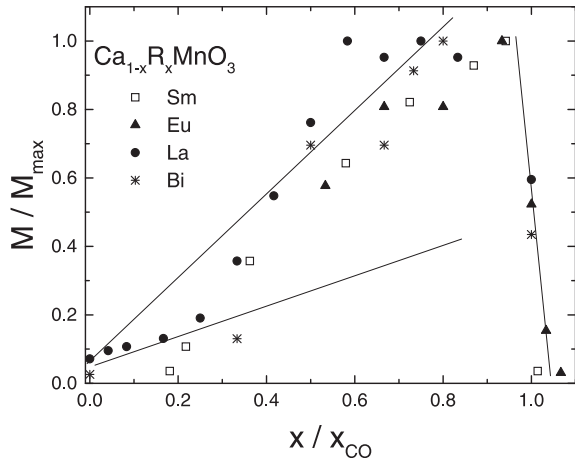


FIG. 10.  $M_0$  vs.  $x$  dependence for  $\text{Ca}_{1-x}\text{R}_x\text{MnO}_3$  for different nonmagnetic R dopants.  $M_0$  and  $x$  are normalized to the  $M_{max}$  and  $x_{CO}$  values as explained in the text.

Our measurements in  $\text{Ca}_{1-x}\text{Y}_x\text{MnO}_3$  show that the magnetic and electrical transport properties share a common behaviour with other  $\text{Ca}_{1-x}\text{R}_x\text{MnO}_3$  with  $\text{R}=\text{Lanthanides}$ , in spite of the important mismatch caused by the small size of  $\text{Y}^{3+}$  ions. To make this point clear, in Fig. 10 we show  $M(5\text{K})$  vs.  $x$ , measured for non magnetic (or weakly magnetic)  $\text{R}^{3+}$  in Refs. 4, 10, 11, 13, and 18. Data are normalized to the charge ordering concentration  $x_{CO}$ , and to the maximum value of  $M(x)$ . This behaviour is coincident with that of Fig. 7 for  $\text{R}=\text{Y}$ : the magnetization rises slowly for small  $x$  and, for  $x/x_{CO} \simeq 0.25$ ,  $M$  increases at larger rate. The net magnetization reached depends on the size of the polarons and of the electron concentration. The dependence found suggests a change of behaviour at  $x \sim 0.03$ . This result confirms that among the three chemical factors governing the CMR properties in doped perovskites: carrier density, average size, and size mismatch, the electron concentration is predominant<sup>4</sup> in electron doped materials. The physical mechanism proposed here can also be applied to the  $M_0(x)$  behaviour in other electron doped manganites with different size of R.

The differential susceptibility, slope of the linear dependence of  $M$  vs.  $H$  in the high field region, results also proportional to the dopant concentration and is, in all cases, larger than the expected value for the  $\text{CaMnO}_3$  background. We can interpret the  $x$  dependence of  $\chi_{diff}$  as a process of enlargement of the polarons with the applied field as suggested by numerical simulations<sup>22</sup>.

In the paramagnetic region we have found that  $\chi^{-1}(T)$  curves deviate substantially from the Curie-Weiss law, showing strong ferromagnetic DE correlations, competing

with the AF interaction of the background material. We discuss our results through a mean field model where FM and AF interactions between  $\text{Mn}^{4+}$  and  $\text{Mn}^{3+}$  are included. From the fits of  $\chi^{-1}(T)$  and using the measured  $T_{mo}$  we obtain values of the parameters of the model, which indicate that the FM-DE interaction is about twice as intense as the AF interaction. The effect of the FM coupling enhances the magnetic moment of the  $\text{Mn}^{3+}$  ions reflecting the magnetic polaron formation, even in the PM phase.

The  $\text{Ca}_{1-x}\text{Y}_x\text{MnO}_3$  conductivity is proportional to the dopant concentration as shown in Fig. 8(b). This dependence precludes the existence of phase separation that would produce a percolative behaviour at a critical concentration. On the other hand, the temperature dependence, for  $T > T_{mo}$ , is of the form  $\sigma(T)=T^{-1}\exp(\Delta/k_B T)$ . This behaviour is compatible with polaronic conductivity.

Summing up, from the magnetic and electric transport properties, we conclude that the electron doped  $\text{CaMnO}_3$  does not show neither phase separation nor homogeneous canted structure. Rather, the results point to the scenario where magnetic or magnetoelastic polarons are responsible for the observed behaviours.

*Acknowledgements* : We acknowledge partial support from ANPCYT (Argentina)-PICT 3-52-1027/3-05266, and CONICET (Argentina)-PIP 4947/96. H. A. is CONICET (Argentina) PhD-fellow.

- 
- <sup>1</sup> C. W. Searle and S. T. Wang, Can. J. Phys. **47**, 2023 (1969).
  - <sup>2</sup> Y. Tokura and Y. Tomioka, J. Mag. Mag. Mat. **200**, 1 (1999).
  - <sup>3</sup> L. M. Rodríguez-Martínez and J. P. Attfield, Phys. Rev B **54**, R15622 (1996).
  - <sup>4</sup> C. Martin, A. Maignan and M. Hervieu, B. Raveau, Phys Rev B **60**, 12191 (1999).
  - <sup>5</sup> E. Dagotto, S. Yunoki, A. L. Malvezzi, A. Moreo, J. Hu, S. Capponi, D. Poilblanc, N. Furukawa, Phys. Rev. B, **58**, 6414 (1998).
  - <sup>6</sup> A. Maignan, C. Martin, F. Damay and B. Raveau, Chem. Mater. **10**, 950 (1998).
  - <sup>7</sup> D. Vega, G. Leyva, G. Polla, P. König, H. Lanza, A. Esteban, H. Aliaga, M. T. Causa, M. Tovar and B. Alascio, J. Solid State Chem., **156**, 458 (2001).
  - <sup>8</sup> H. Aliaga, M. T. Causa, B. Alascio, H. Salva, M. Tovar, D. Vega, G. Polla, G. Leyva and P. König, J. Mag. Mag. Mat. (in press).
  - <sup>9</sup> C. D. Batista, J. Eroles, M. Avignon and B. Alascio, Phys. Rev. B **58**, R14689 (1998).
  - <sup>10</sup> I. O. Troyanchuk, H. Szymczak and A. Nabialek, J. Solid State Chem. **131**, 144 (1997).
  - <sup>11</sup> J. J. Neumeier and J. L. Cohn. Phys. Rev. B, **61**, 21, 14319 (2000).

- <sup>12</sup> J. J. Neumeier and D. G. Goodwin, *J. Applied Phys.* **85**, 5591 (1999).
- <sup>13</sup> H. Chiba, M. Kikuchi, J. Kusaba, Y. Muraoka, and Y. Syono, *Solid State Phys.* **85**, 499 (1996).
- <sup>14</sup> D. L. Huber, A. Alejandro, A. Caneiro, M. T. Causa, F. Prado, M. Tovar and S. B. Oseroff, *Phys. Rev. B* **60**, 12155 (1999).
- <sup>15</sup> E. O. Wollan and W. C. Kohler, *Phys. Rev.* **100**, 545 (1955).
- <sup>16</sup> G. H. Jonker, *Physica* **22**, 707 (1956); V. M. Yudin, A. I. Gavrilishina, M. V. Artemeva and M. F. Bryshina, *Sov. Phys. Solid State* **7**, 8 (1966); J. Briatico, B. Alascio, R. Allub, A. Butera, A. Caneiro, M. T. Causa and M. Tovar, *Phys. Rev. B* **53**, 14020 (1996).
- <sup>17</sup> C. Zener, *Phys. Rev.* **82**, 403 (1951); P. W. Anderson and H. Hasegawa, *Phys. Rev.* **100**, 675 (1955).
- <sup>18</sup> P. N. Santosh, J. Goldberger, P. M. Woodward, T. Vogt, W. P. Lee, and A. J. Epstein. *Phys. Rev. B* **62**, 14928 (2000).
- <sup>19</sup> J. van den Brink and D. Khomskii, *Phys. Rev. Letters* **82**, 1016 (1999).
- <sup>20</sup> R. Kajimoto, H. Yoshizawa, H. Kawano, H. Kuwahara, Y. Tokura, K. Ohoyama, and M. Ohashi. *Phys. Rev. B* **60**, 9506 (1999).
- <sup>21</sup> R. Mahendiran, A. Maignan, C. Martin, M. Hervieu, and B. Raveau. *Phys. Rev. B* **62**, 11644 (2000).
- <sup>22</sup> H. Aliaga, private communication.